ASIAN JOURNAL OF PHARMACEUTICAL AND CLINICAL RESEARCH

INNOVARE ACADEMIC SCIENCES
Knowledge to Innovation

Vol 12, Issue 6, 2019

Online - 2455-3891
Print - 0974-2441

Research Article

PHYSICAL AND CHEMICAL CHARACTERIZATION OF GREEN SYNTHESIZED SILVER NANOPARTICLES USING STEM OF *HIBISCUS VITIFOLIUS* L. AND ITS ANTIMICROBIAL AND ANTIOXIDANT POTENTIAL

ANTONY LAWRENCE A, THOMAS JOSEPH PRAKASH J*

Department of Physics, Government Arts College (Affiliated to Bharathidasan University), Tiruchirappalli, Tamil Nadu, India.

Email: armyjpr1@yahoo.co.in

Received: 17 March 2019, Revised and Accepted: 15 April 2019

ABSTRACT

Objectives: The aim of our work was to synthesize the silver nanoparticle (AgNP) using *Hibiscus vitifolius* L. stem extract its characterization and evaluation of antimicrobial and antioxidant assay.

Materials and Methods: The silver nitrate (1 mM) mixed with aqueous stem extract of *H. vitifolius* L. after the nanoparticles is examined by Fourier-transform infrared (FT-IR), ultraviolet-visible (UV-vis) spectroscopy, field emission scanning electron microscopy (FE-SEM), energy-dispersive X-ray (EDAX), X-ray powder diffraction (XRD), dynamic light scattering (DLS), zeta potential, thermogravimetry/differential thermal analysis (TG/DTA), and differential scanning calorimetry (DSC). The aqueous stem extract is examined for phytochemical screening, gas chromatography–mass spectrometry (GC–MS) analysis, FT-IR, and UV-vis spectroscopy. The antibacterial, antifungal, and antioxidant assay were also evaluated for the AgNPs.

Results: The aqueous stem extract shows 20 compounds in GC–MS analysis. The FT-IR and UV-vis spectroscopy show the biocompounds. *H. vitifolius* stem extract-AgNPs (HVS-AgNPs) examined in UV and FT-IR shows the presence of AgNPs, FE-SEM shows that the particle size is 30–70 nm, EDAX shows the presence of silver metal, and XRD shows that the particles are face-centered cubic. DLS shows the hydrodynamic size 136.9 nm, zeta potential shows the stability (−18.6 mV), and TG/DTA and DSC show that the particles are stable up to 335°C. The HVS-AgNPs are also evaluated in antimicrobial and antioxidant potential and the report shows a good inhibition.

Conclusion: The stem extract of *H. vitifolius* L. can be used for green synthesis of AgNPs and could be used as antimicrobial and antioxidant potential.

Keywords: Antimicrobial activity, Antioxidant assay, Characterization, *Hibiscus vitifolius* L., Silver nanoparticles.

 DOI: http://dx.doi.org/10.22159/ajpcr.2019.v12i6.33113

INTRODUCTION

Due to the multiplicative property of nanomaterials, they are undergone to intense research. Research in academic and engineering, metal nanoparticles have novel physical and chemical properties [1-13]. Nanomaterials are strongly depending on properties such as shape, size, and surface nature [14-16]. To adjust these properties, numerous strategies are used such as a chemical reduction method, chemical vapor deposition, electrodeposition, lithography, laser ablation, and sol-gel technique [14, 17-21]. Among these, the chemical reduction method is highly implied, but unfortunately, it is highly toxic which limits the silver nanoparticles (AgNPs) application [22-24]. To avoid the toxicity and to be friendly with the environment, we use green chemistry approach of synthesis using plants and microbes. This form of synthesis is simple, rapid, and ecofriendly. The green chemical method is budding approach in nanotechnology [25,26]. In this green chemical method, it is deducted that extraction of living organisms acts as capping and reducing agent to synthesize nanoparticles [27]. Thus, the quality of plant extract is of high importance [28,29].

In our present work, we aim to synthesize the AgNPs using *Hibiscus vitifolius* stem extract and is characterized by various techniques such as Fourier-transform infrared (FT-IR), ultraviolet-visible (UV-vis) spectroscopy, field emission scanning electron microscopy (FE-SEM), energy-dispersive X-ray (EDAX), X-ray powder diffraction (XRD), dynamic light scattering (DLS), zeta potential and thermally examined by TG-DTA, and differential scanning calorimetry (DSC) for the AgNPs. The aqueous stem extract is also examined by UV-vis spectroscopy, FT-IR, gas chromatography–mass spectrometry (GC–MS), and phytochemical screening. Finally, the AgNPs are evaluated by antioxidant and antimicrobial studies. This shows the positive result in its application.

MATERIALS AND METHODS

Silver nitrate, chemicals, and other solvents (AR grade) were drawn from Sigma-Aldrich, India. *H. vitifolius* L. stem was collected in Tiruchirappalli and dedicated in Rapinat Herbarium, St. Joseph College, Tiruchirappalli, India (Voucher No: AAL 002) shown in Fig. 1.

Preparation of stem extract

The drawn stem of *H. vitifolius* L. was washed with water and rinsed with double distilled water. The rinsed stem was dried in room for 2 weeks. Then, it is grained using pestle mortar. 10 g of stem powder were weighted and soaked in 100 ml of double distilled water in a 250 ml beaker for 30 min. After then, it is boiled at 70°C for 20 min. Then, the cooled extract is filtered using Whatman No 1 filter paper and the final extract is stored at 4°C.

Phytochemical screening and GC–MS evaluation

The aqueous extract of the stem is evaluated by phytochemical screening. The screening was performed for the following compounds such as a glycoside, xanthoprotein, coumarin, phenols, emodin, alkaloids, tannin, carbohydrates, saponin, phlobatanin, saponin, flavonoids, steroids, terpenoids, leucoanthocyanin, cardiac glycoside, anthocyanin, protein, and anthraquinone [30,31]. The stem extract is also examined by GC–MS analysis.

Preparation of silver nanoparticles and its characterization

Silver nitrate solutions 1 mM (120 ml) are prepared and add 6 ml of stem extract for biosynthesis process [32]. The color change is

observed from yellow to dark brown after a day. This change in color is an identity that the AgNPs is formed, Fig. 2. Then, it is centrifuged (Remi RM-12C) at 12,000 rpm. The product is dried and purified by alcohol twice and further, it is dried using the air hot oven. The final powder is characterized by different techniques using the instrument as shown in Table 1.

Antimicrobial assays

Collection of bacterial strain

H. vitifolius stem extract-AgNPs (HVS-AgNPs), *H. vitifolius* stem extract, $AgNO_3$, and amoxicillin (standard) are undergone for antibacterial assay. From microbial type culture and collected MTCC, Chandigarh, India, the bacterial strains *Staphylococcus aureus* (MTCC 25923), *Bacillus subtilis* (MTCC 2451), *Escherichia coli* (MTCC 25922), and *Pseudomonas aeruginosa* (MTCC 27853) were collected. These bacterial strains were cultured at 37°C and placed on nutrient agar (Difco, USA) stored at 4°C.

Table 1: Instrument model and its uses

Instrument and model	Application
UV-visible spectroscopy (U-2910 Hitachi)	Optical studies
FT-IR (IRAffinity-1S Shimadzu)	Functional group identification
FE-SEM (JEOL JSM-6701F)	Surface morphology studies
EDAX (INCA Penta FETX3 OXFORD)	Elemental analysis
XRD (X'Pert Pro-P Analytic)	Lattice parameter
DLS, zeta potential (Malvern Zetasizer, Nano ZS90)	Particle size, stability
GC–MS (SHIMADZU QP 2010Plus)	Identify chemical compounds
TG/DTA (DT Q600 V20.9 Build 20)	Thermal *analysis*
DSC (NETZSCH DSC 214 Polyma)	Properties of material

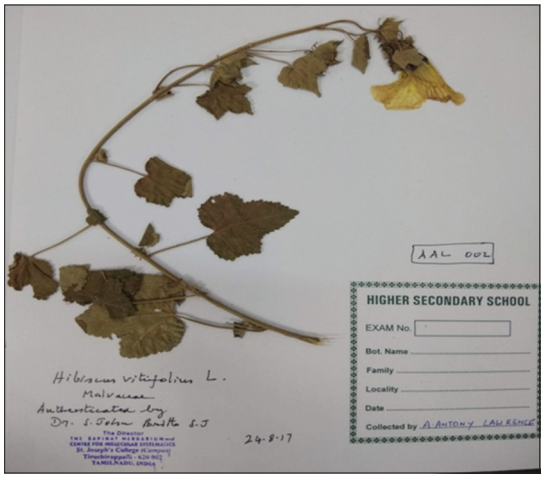

Fig. 1: *Hibiscus vitifolius* L. identified in Rapinat Herbarium (Voucher No: AAL 002)

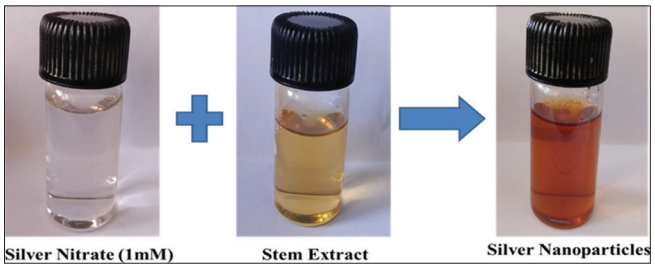

Fig. 2: Silver nitrate solution mixed with *Hibiscus vitifolius* stem extract gives silver nanoparticles

Antibacterial screening

The HVS-AgNPs, *H. vitifolius* stem extract, $AgNO_3$, and amoxicillin (standard) are evaluated antibacterial by disk diffusion method. The Mueller-Hinton agar is prepared and poured in Petri dishes (60 mm) after it is inoculated with testing organisms. The sterile disk (6 mm width) was impregnated with 10 µl samples, then placed on the top layer of the Petri dish. Then, the disk is then incubated for 24 h at 37°C and the zone of inhibition is recorded [33].

Collection of fungal strain

Two different fungal strains (*Candida albicans* [MTCC-3498] and *Aspergillus niger* [MTCC-227]) were collected from Natural Chemical Laboratory, Pune, Maharashtra, India. They were separately incubated by Sabouraud's dextrose broth for 6 h and are checked to provide approximately 10^5 CFU/ml.

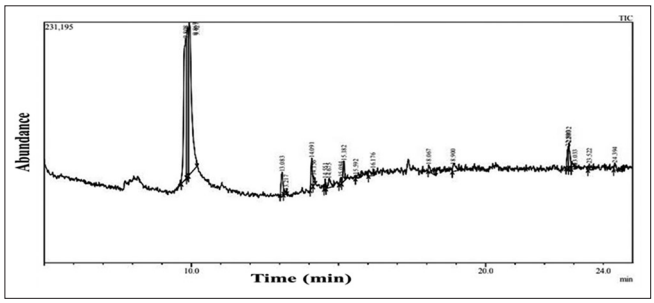

Fig. 3: Gas chromatography–mass spectrometry analysis of *Hibiscus vitifolius* aqueous stem

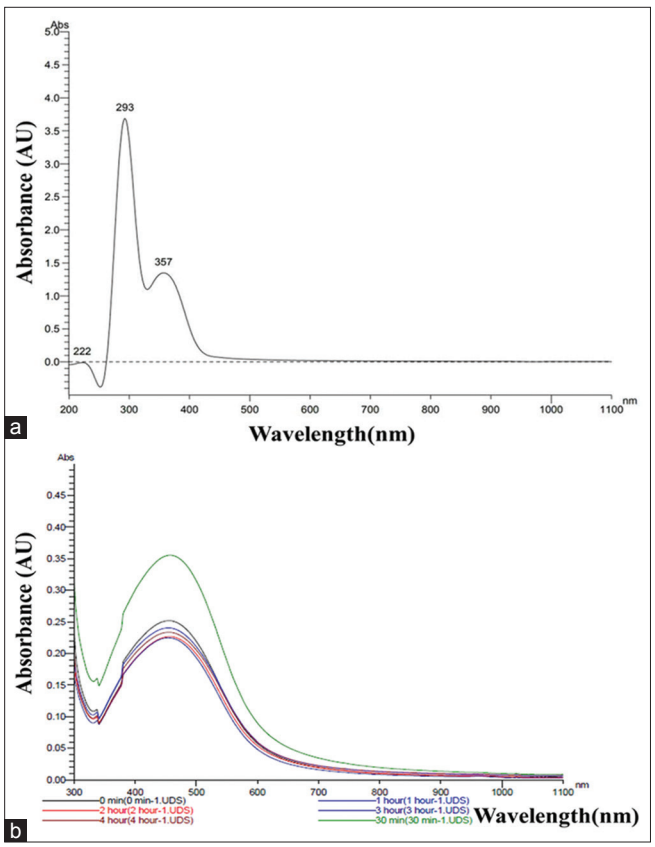

Fig. 4: Ultraviolet-visible spectroscopy of (a) *Hibiscus vitifolius* aqueous stem extract. (b) HVS-AgNPs in increasing order during different time period (Black – 0 min, Green – 30 min, Light blue – 1 h, Red – 2 h, Blue – 3 h, and Maroon – 4 h)

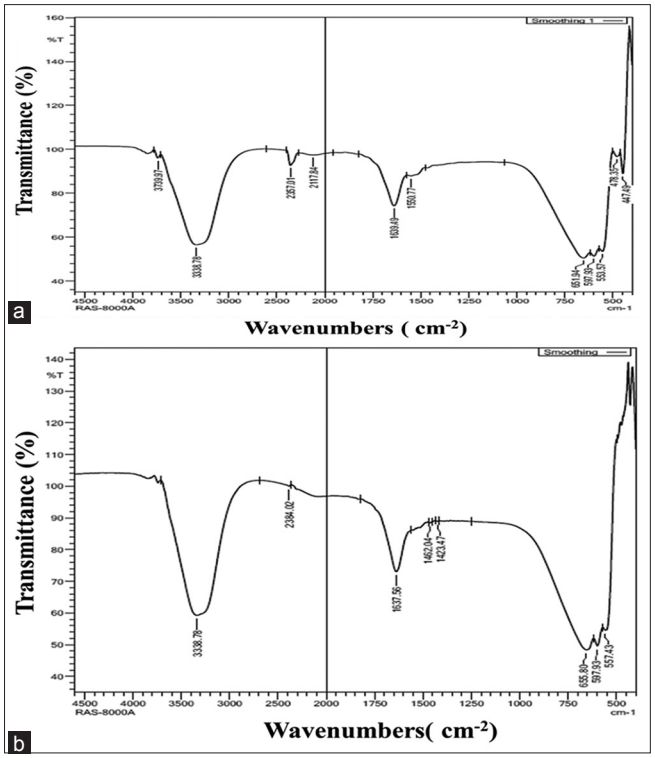

Fig. 5: Fourier-transform infrared spectroscopy of (a) *Hibiscus vitifolius* aqueous stem extract and (b) HVS-AgNPs

Antifungal screening

The Sabouraud's dextrose agar is prepared and poured in Petri dishes (60 mm) after it is inoculated with testing organisms. The sample (HVS-AgNPs, *H. vitifolius* stem extract, $AgNO_3$, and *Fluconazole* [standard]) is impregnated with 10 µl in sterile disk (6 mm) and placed on top of Petri dishes. The disk is then incubated for 24 h at 37°C after inhibition is recorded.

Antioxidant in vitro

2,2-diphenyl-2-picrylhydrazyl (DPPH) is used for free radical scavenging activity. The DPPH radicals (0.2 mM) are prepared using methanol solution. HVS-AgNPs (20–100 µg/ml) in water were mixed with 1 ml of prepared DPPH solution. The solution is taken in a test tube and shaken vigorously after the test tube is placed 30 min in dark room. Then, absorbance is measure. Similarly, ascorbic acid is used as standard and is compared with the HVS-AgNPs. After measuring, the IC_{50} value is calculated [34].

The scavenging ability is calculated using formula.

$$\% \text{ of inhibition} = 100\times \left(\frac{A-B}{A}\right)$$

Where, I (%) is inhibition percentage
- *A*: Absorbance of control reaction
- *B*: Sample absorbance of test compound.

RESULTS AND DISCUSSION

Examination of stem aqueous extract

The dried material phytochemicals are more active and are more concentrated than that of fresh materials [35,36]. The synthesis is uniform and rapid in dried materials when compared to fresh materials.

Table 2: Gas chromatography–mass spectrometry analysis of *Hibiscus vitifolius* aqueous stem extract

Peak	Retention time	Area%	Height%	A/H	Name	Molecular weight	Formula
1	9.808	26.72	21.83	6.52	Bis (1-methyl-4-pentenyl) phthalate	330	$C_{20}H_{26}O_4$
2	9.867	17.08	23.33	3.90	1,2-Benzenedicarboxylic acid, mono (phenylmethyl) ester	256	$C_{15}H_{12}O_4$
3	9.927	31.32	23.72	7.03	1,2-Benzenedicarboxylic acid, diethyl ester	222	$C_{12}H_{14}O_4$
4	13.083	2.65	3.52	4.01	1,2-Benzenedicarboxylic acid, mono butyl ester	222	$C_{12}H_{14}O_4$
5	13.217	0.53	0.57	4.97	Propane, 2,2-difluoro	80	$C_3H_6F_2$
6	14.091	2.84	4.65	3.24	1,2-Benzenedicarboxylic acid, 2-butoxyethyl ester	322	$C_{18}H_{26}O_5$
7	14.156	0.80	1.50	2.83	1,2,4-Butanetriol	106	$C_4H_{10}O_3$
8	14.551	0.64	1.55	2.18	Pentanoic acid, 3-methyl	116	$C_6H_{12}O_2$
9	14.675	1.68	1.36	6.56	3-Butene-1,2-diol, 1-(2-furanyl)	154	$C_8H_{10}O_3$
10	15.084	0.61	1.05	3.12	2-Methyl-2,3-epoxyl-1-propanol	88	$C_4H_8O_2$
11	15.182	2.61	3.15	3.65	1-Tetradecanol	214	$C_{14}H_{30}O$
12	15.592	0.73	0.56	7.01	1,2-Ethanediol, monofomate	90	$C_3H_6O_3$
13	16.176	1.15	1.06	5.78	2-Amino-2-methyl-1,3-propanediol	105	$C_4H_{11}NO_2$
14	18.067	1.70	1.07	8.47	Hexanal	100	$C_6H_{12}O$
15	18.900	1.55	1.05	7.87	Cyclohexane, 1-ethyl-2-methyl-, cis	126	C_9H_{18}
16	22.800	2.15	3.42	3.35	1-Butanol, 3-methyl	88	$C_5H_{12}O$
17	22.832	2.29	3.99	3.05	Hexanoic acid, 2-methyl	130	$C_7H_{14}O_2$
18	23.033	1.04	0.58	9.48	Pentanoic acid	102	$C_5H_{10}O_2$
19	23.522	0.92	0.92	5.34	2-Propanamine, 1-(2,6-dimethylphenoxy)	179	$C_{11}H_{17}NO$
20	24.394	1.45	1.10	7.00	Ethanol, 2-[(2-aminoethyl) amino]	104	$C_4H_{12}N_2O$
-		100	100				

Table 3: Zone of inhibition of MHS-silver nanoparticles, stem extract, $AgNO_3$, and standard against various microbes

	HVS-AgNPs (D)	Stem extract (C)	$AgNO_3$(A)	Standard (B) amoxicillin/fluconazole
Staphylococcus aureus (MTCC 25923)	5.12 ± 0.012	2.04 ± 0.016	0	8.17 ± 0.031
Bacillus subtilis (MTCC 2451)	6.05 ± 0.017	3.12 ± 0.025	0	8.16 ± 0.023
Escherichia coli (MTCC 25922)	6.12 ± 0.020	4.31 ± 0.017	0	8.21 ± 0.019
Pseudomonas aeruginosa (MTCC 27853)	3.23 ± 0.026	2.09 ± 0.022	0	8.09 ± 0.027
Candida albicans (*MTCC*-3498)	3.19 ± 0.021	2.16 ± 0.014	0	8.23 ± 0.016
Aspergillus niger (MTCC-227)	4.17 ± 0.016	3.13 ± 0.018	0	8.13 ± 0.014

*All the experiments were repeated independently 3 times and the values were represented as an average means ± SD. SD: Standard deviation, AgNPs: Silver nanoparticles, HVS: *Hibiscus vitifolius* stem extract

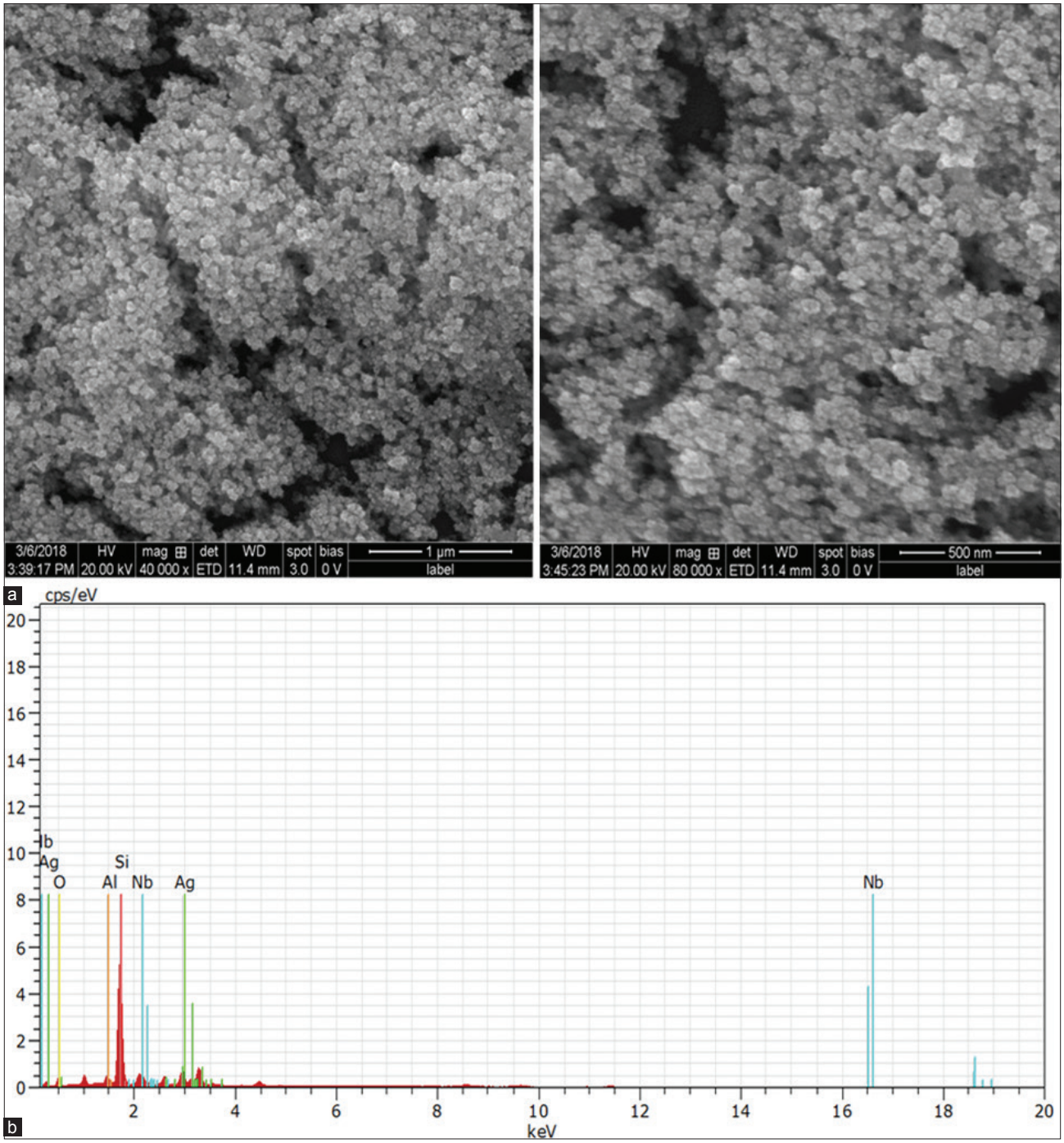

Fig. 6: (a) Field emission scanning electron microscopy image of HVS-AgNPs and (b) energy-dispersive spectroscopy spectrum of HVS-AgNPs

Phytochemical screening

The biocompounds were identified by phytochemical screening. The screening report project the presents of phenols, coumarin, xanthoprotein, emodin, alkaloids, phlobatanin, flavonoids, tannin, saponin, steroid, protein, anthroquinon and cardiac glycoside. The compounds such as glycoside,leucoanthocyanin, carbohydrate, terpenoid, and anthocyanin are absent.

GC–MS analysis

H. vitifolius aqueous stem extract shows 20 compounds and was identified in GC–MS analysis. The compounds were identified by NIST/WILEY spectral database and data are given in Table 2 and Fig. 3. In GC–MS, there are three major compounds 1,2-benzenedicarboxylic acid, diethyl ester, Bis (1-methyl-4-pentenyl) phthalate, and

Table 4: Free radical scavenging activities (2,2-diphenyl-2-picrylhydrazyl method) of *Hibiscus vitifolius* stem extract-silver nanoparticles and ascorbic acid

Concentration of AgNPs (µg/ml)*	HVS-AgNPs	Ascorbic acid
20	54.06±0.007	86.43±0.007
40	56.50±0.009	87.63±0.007
60	62.60±0.011	90.45±0.060
80	67.07±0.005	93.59±0.001
100	69.91±0.009	96.34±0.010

*All the experiments were repeated independently 3 times and the values were represented as an average means±SD. SD: Standard deviation, AgNPs: Silver nanoparticles, HVS: *Hibiscus vitifolius* stem extract

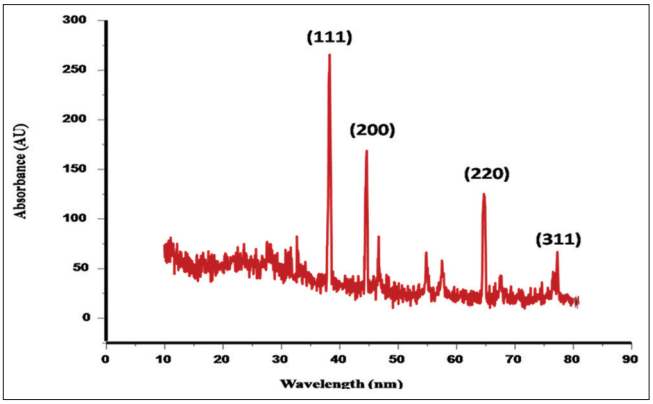

Fig. 7: X-ray powder diffraction of HVS-AgNPs

1,2-benzenedicarboxylic acid, mono(phenylmethyl) ester at retention time 9.927, 9.808, and 9.867, respectively. These compounds play an active role to synthesis AgNPs.

UV-vis and FT-IR spectroscopy

The UV range for aqueous stem extract is 222, 293, and 357 nm in UV-vis spectroscopy this denotes the presences of flavonoids as shown in Fig. 4a. Fig. 5a shows that FT-IR of *H. vitifolius* stem extract has various peaks at 3739.97 cm^{-1} (O-H stretching vibration), 3338.78 cm^{-1} (tertiary amine N-H stretching vibration resembles carboxylic acids), 2357.01 cm^{-1} (C = N), 1639.49 cm^{-1} (carbon bond C = C stretching vibration), and 651.94 cm^{-1} (C-Br alkyl group). 1639.49 cm^{-1} peak is evident of the phenyl group by the O-H bond stretching along with sp2 carbon bond stretching C = C. This phenyl group corresponds in GC–MS analysis.

Examination of silver nanoparticles

The basic technique used for characterizing the AgNPs is UV-vis spectroscopy. The color arises due to the excitation of surface plasmon vibration in AgNPs [37]. The absorption band at 425–450 nm indicates that the AgNPs are spherical shaped [38]. The absorption band for HVS- AgNPs is at 440–446 nm and is observed for different interval of time such as 0 min, 30 min, 1 h, 2 h, 3 h, and 4 h as in Fig. 4b. The red shift of nanoparticles is due to the modification in shape and size [23]. In *Aegle marmelos* leaf extract, AgNP shows the spectral studies close to 450 nm this confirms the formation of AgNPs and this absorption depends on dielectric medium, particle size, and chemical surrounding [39]. The FT- IR for HVS-AgNPs shows various peaks at 3338.78 cm^{-1} (N-H stretching vibration), 2384.02 cm^{-1} (O-H stretching vibration), 1637.56 cm^{-1} (C = C carbon bond stretching vibration), and 655.80 cm^{-1} (C-Br alkyl group). The presence of NO^2 in fingerprint region (1500 cm^{-1}–1000 cm^{-1}). The two groups (N-H and C = N) are actively participating in the reduction of HVS-AgNPs as are evident by shifting of peaks as shown in Fig. 5b.

The FE-SEM and EDAX were used to study the morphology, size, and elemental composition of biosynthesized AgNPs. The synthesized nanoparticles at micro (10^{-6}) and nano (10^{-9}) can be identified by FE- SEM. The surface imaging technique, detection of particle shape, size, surface morphology and size distribution of nanoparticles [40-42]. The FE-SEM clearly shows that the particle is spherical and the size is found to be about 30–70 nm for HVS-AgNPs as shown in Fig. 6a. The size of particles matches with *Tamarindus indica* seed coat AgNPs [43]. The elemental composition of AgNPs is examined by EDAX spectroscopy and is a chemical analysis method combined with the FE-SEM [44]. In EDAX, the optical absorption peak at 3 KeV is observed, this shows that metallic silver nanocrystallites which are due to surface plasmon resonance [45]. The other element signals are due to phytochemicals or the protein present in stem extract and Si element is due to the glass wafer used for coating AgNPs shown in Fig. 6b.

The XRD peak depicts clearly that the AgNPs are crystalline in nature. From Fig. 7, the XRD pattern shows four distinct diffraction peaks at 38.2°C, 44.6°C, 64.7°C, and 77.3°C for indexing planes (111), (200), (220), and (311), respectively. These marked indices confirm that the sample is metallic AgNPs and is face-centered cubic crystal structure (JCPDS No. 04-0873). The peak at 38.2°C pertaining to (111) diffraction peak and is more intense peak than other. There are small other peaks which are due to biomolecules of *H. vitifolius* stem extract adsorbed on AgNPs. The AgNPs mean crystallite size was measured by the Debye-Scherrer method. $D = K\lambda/\beta \cos\theta$ (K – Scherrer constant, related to crystalline shape, λ –Radiation wavelength, β – Full width at half maximum of the diffraction peak, and θ – Bragg's angle). The average crystallite size of AgNPs was 40 nm.

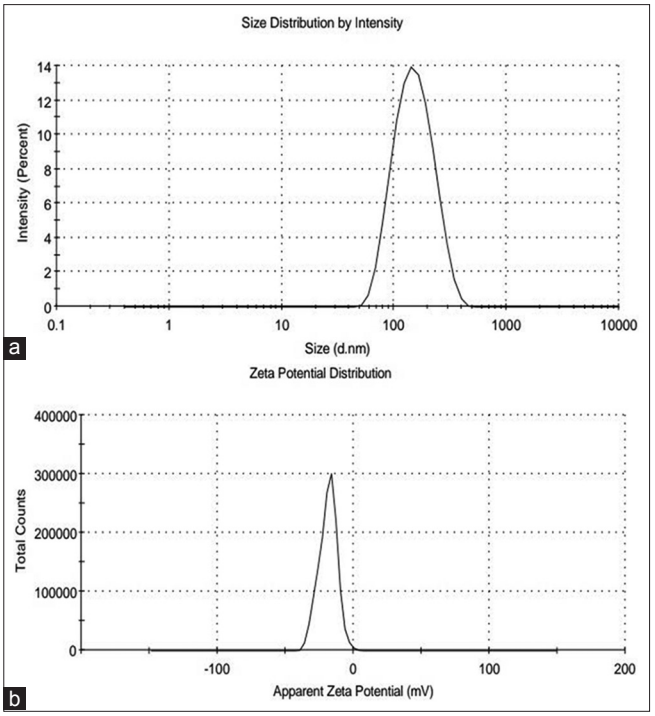

Fig. 8: (a) The hydrodynamic size of HVS-AgNPs and (b) zeta potential of HVS-AgNPs

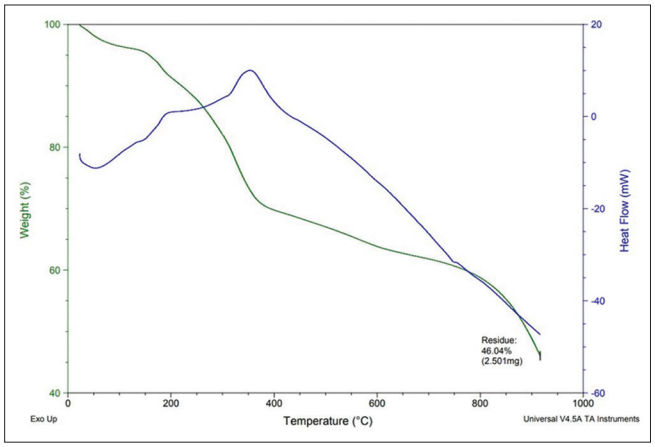

Fig. 9: Thermogravimetry/differential thermal analysis of HVS-AgNPs

From DLS analysis, the average hydrodynamic size and zeta potential of HVS-AgNPs were observed. The size distribution graph of HVS-AgNPs shows a single peak between 63.47 nm and 159.2 nm and its average size was found to be 136.9 nm shown in Fig. 8a. This matches with *Momordica charantia* fruit AgNPs [46]. Since DLS is measured based on hydrodynamic diameter, the particle size is big compared to FE-SEM.

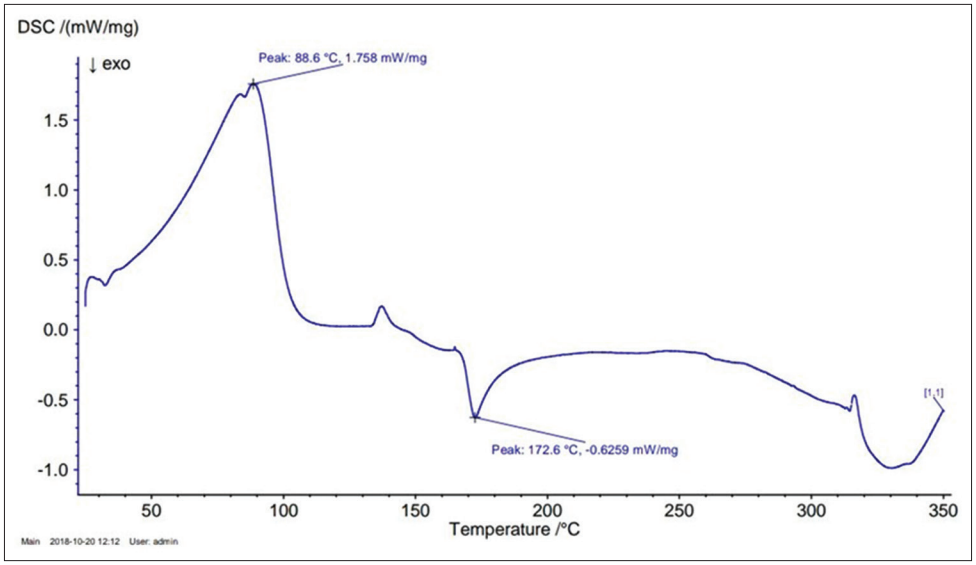

Fig. 10: Differential scanning calorimetry of HVS-AgNPs

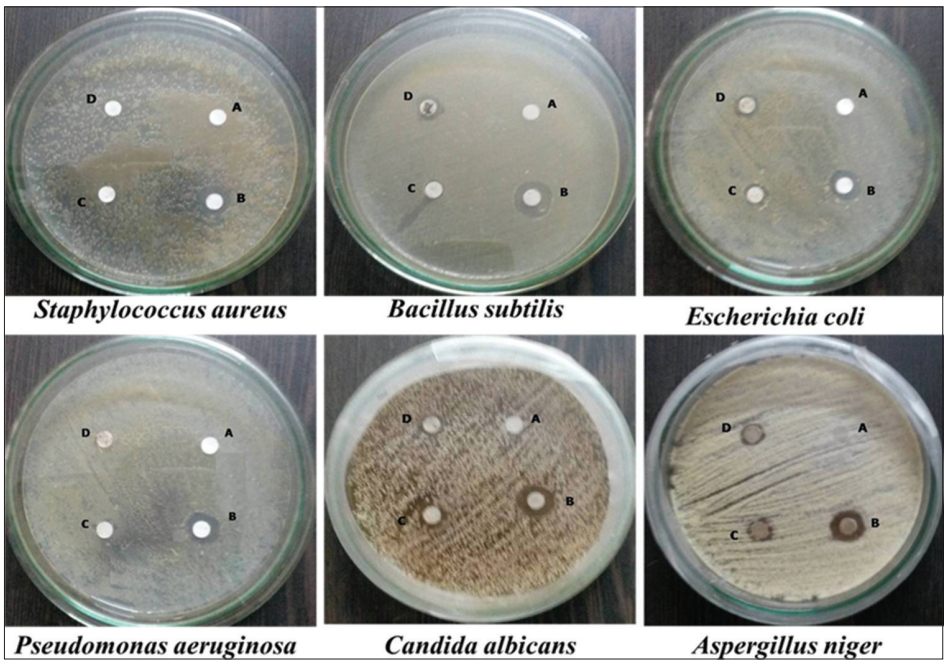

Fig. 11: Zone of inhibition of HVS-AgNPs, stem extract, $AgNO_3$, and standard for various antibacterial and antifungal strains

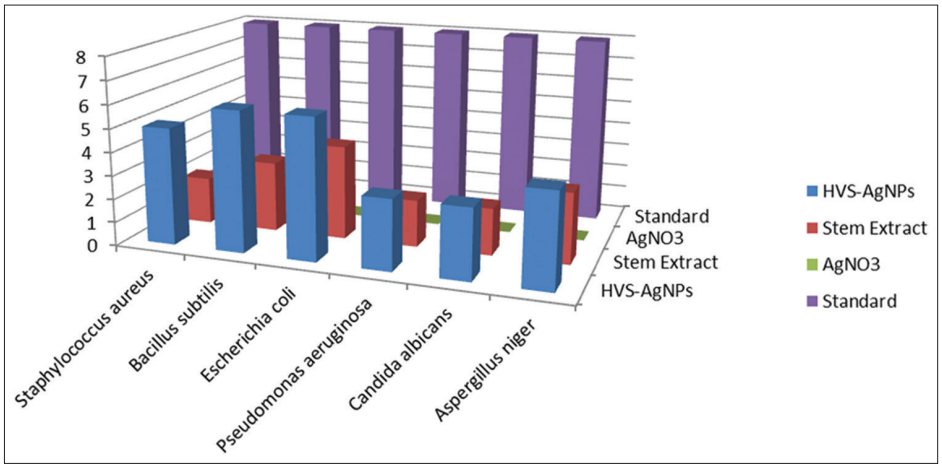

Fig. 12: Zone of inhibition of antimicrobial activity represented in bar chart

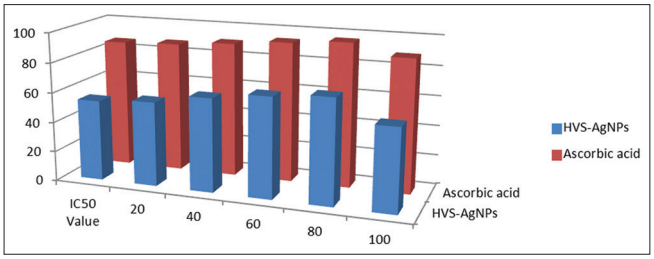

Fig. 13: Antioxidant activity (2,2-diphenyl-2-picrylhydrazyl method) represented in bar chart

The zeta potential of HVS-AgNPs was found to be −18.6 mV as shown in Fig. 8b. In dispersion medium, the negative value of zeta potential shows that the HVS-AgNPs are highly stable and have a strong repellent force within the particles and it also prevents aggregation [47,48].

The thermal stability of HVS-AgNPs was examined by thermogravimetry/differential thermal analysis (TG/DTA). In TG curve, we observe weight lost from 5.4330 mg (room temperature) to 2.501 mg (920°C) and the residue is 46.04% after 920°C it is constant there is no weight loss. The weight is been lost at five stages from room temperature to 160.79°C, 160.79°C to 358.11°C, 358.11°C to 583.09°C, 158.09°C to 834.62°C, and 834.62°C to 920°C. The primary weight loss is mainly due to moisture content present in AgNPs. The major weight losses occur at 160.79°C–358.11°C. The decomposition of materials produces the weight loss of AgNPs. In DTA curve, we observe endothermic peak at 55°C and two exothermic peaks at 210°C and 350°C show that melting point of AgNPs. The energy is been released at 350°C as depicted in DTA curve shown in Fig. 9. Using DTA, we examine the crystallinity and thermal decomposition of AgNPs [49].

From the DSC curve, we observe three exothermic peaks at 88°C, 172.6°C, and 335°C. During these exothermic peaks, the energy is been released from the materials. The peak at 335°C shows that the material melts at this stage, and hence, they are stable until 335°C. We also observe three endothermic peaks at 88.6°C, 136°C, and 317°C during this stage, the energy is been absorbed by materials. These exothermic peaks and endothermic peak lie on glass transition, crystalline, and melting stages. They are due to changes in properties of materials. There are also small other peaks present in the DSC curve shown in Fig. 10.

Antimicrobial screening

The HVS-AgNPs showed good inhibition action of bacteria such as *B. subtilis* (6.05 ± 0.017 mm), *E. coli* (6.12 ± 0.020 mm), *S. aureus* (5.12 ± 0.012 mm), and *P. aeruginosa* (3.23 ± 0.026 mm) and a small inhibition for stem extract shown in Figs. 11 and 12 and Table 3. These values are compared with amoxicillin (standard). These HVS-AgNPs show a moderate inhibition for fungal stains such as *A. niger* (4.17 ± 0.016 mm), *C. albicans* (3.19 ± 0.021 mm), and small inhibition for stem extract, these values are compared with *Fluconazole* (standard). There is no inhibition for silver nitrate solution (1 mM) for both antibacterial and antifungal assay.

Free radical scavenging activity (DPPH method)

The free radical scavenging activity (DPPH method) was evaluated for HVS-AgNPs for different concentrations from 20 µg/ml to 100 µg/ml. They show a good antioxidant property for AgNPs and are alternately compared with the ascorbic acid standard. Since HVS-AgNPs is prepared naturally, they are non-toxic and have no side effect when compared with the standard. The IC_{50} value is calculated as shown in Fig. 13 and Table 4.

CONCLUSION

The green synthesis method is cost effective, ecofriendly, and easy method to execute. The physical and chemical property of a material is examined. The physical property such as particle size is 30–60 nm in FE-SEM and 136.7 nm in DLS. They are also examined chemically by FT-IR, EDAX, and XRD, they show the presence of AgNPs. They are also examined by various studies such as TG/DTA and DSC the decomposition of material and the stability was examined by zeta potential. The HVS-AgNPs are also underwent in antimicrobial and antioxidant assay and show good potential. Hence, the synthesized nanoparticles can be well-applied pharmaceutically.

AUTHORS' CONTRIBUTIONS

The authors would like to express our thanks to Dr. J. Thomas Joseph Prakash, Department of Physics, Government Arts College, Tiruchirappalli-22, for providing the infrastructure facility and support.

CONFLICTS OF INTEREST

The authors declare that there are no conflicts of interest regarding the publication of this paper.

REFERENCES

1. Zhang D, Yang H. Gelatin-stabilized copper nanoparticles: Synthesis, morphology, and their surface-enhanced Raman scattering properties. Phys B Condens Matter 2013;415:44-8.
2. Li D, Ma J, Zhou L, Li Y, Zou C. Synthesis and characterization of Cu2S nanoparticles by diethylenetriamine-assisted hydrothermal method. Optik Int J Light Electron Opt 2015;126:4971-3.
3. Huang J, Mao P, Ma P, Pu Y, Chen C, Xia Z. The thermal stability mechanism of gold nanorods in aqueous solution. Optik Int J Light Electron Optics 2016;127:10343-7.
4. Augustine AK, Nampoori VP, Kailasnath M. Rapid synthesize of gold nanoparticles by microwave irradiation method and its application as an optical limiting material. Optik Int J Light Electron Optics 2014;125:6696-9.
5. Li Y, Huo Y, Li C, Xing S, Liu L, Zou G. Thermal analysis of Cu-organic composite nanoparticles and fabrication of highly conductive copper films. J Alloys Compd 2015;649:1156-63.
6. Zhou K, Dong C, Zhang X, Shi L, Chen Z, Xu Y, Cai H. Preparation and characterization of nanosilver-doped porous hydroxyapatite scaffolds. Ceram Int 2015;41:1671-6.
7. Dong C, Zhang X, Cai H, Cao C. Sodium alginate mediated route for the synthesis of monodisperse silver nanoparticles using glucose as reducing agents. Rare Metal Mater Eng 2016;45:261-6.
8. Dong C, Cai H, Zhang X, Cao C. Synthesis and characterization of monodisperse copper nanoparticles using gum acacia. Physica E Low Dimens Syst Nanostruct 2013;57:12-20.
9. Tang XF, Yang ZG, Wang WJ. A simple way of preparing high-concentration and high-purity nano copper colloid for conductive ink in inkjet printing technology. Colloids Surfaces A Physicochem Eng Aspects 2010;360:99-104.
10. Siddiqui H, Qureshi MS, Haque FZ. Surfactant assisted wet chemical synthesis of copper oxide (CuO) nanostructures and their spectroscopic analysis. Optik Int J Light Electron Optics 2016;127:2740-7.
11. Xiong Z, Dong C, Cai H, Liu C, Zhang X. Composite inks of poly (3,4ethylenedioxythiophene)/poly (styrenesulfonate)/silver nanoparticles and electric/optical properties of inkjet-printed thin films. Mater Chem Phys 2013;141:416-22.
12. Philip D. Mangifera indica leaf-assisted biosynthesis of well-dispersed silver nanoparticles. Spectrochim Acta A Mol Biomol Spectrosc 2011;78:327-31.
13. Philip D. Honey mediated green synthesis of silver nanoparticles. Spectrochim Acta A Mol Biomol Spectrosc 2010;75:1078-81.
14. Xu G, Qiao X, Qiu X. Green synthesis of highly pure nano-silver sols-electrolysis. Rare Metal Mater Eng 2013;42:249-53.
15. Jose M, Dhas SA, Daisy AD, Das SJ. Synthesis and characterization of nano spheres decorated silver bromide nanorods using a two step chemical reduction route. Optik Int J Light Electron Optics 2016;127:8019-23.
16. Vidya H, Kumara Swamy BE, Schell M. One step facile synthesis of silver nanoparticles for the simultaneous electrochemical determination of dopamine and ascorbic acid. J Mol Liq 2016;214:298-305.
17. Byeon JH, Kim YW. A novel polyol method to synthesize colloidal silver nanoparticles by ultrasonic irradiation. Ultrason Sonochem 2012;19:209-15.
18. Eluri R, Paul B. Microwave assisted greener synthesis of nickel

nanoparticles using sodium hypophosphite. Mater Lett 2012;76:36-9.
19. Basuny M, Ali IO, El-Gawad AA, Bakr MF, Salama TM. A fast green synthesis of Ag nanoparticles in carboxymethyl cellulose (CMC) through UV irradiation technique for antibacterial applications. J Sol Gel Sci Technol 2015;75:530-40.
20. Wang X, Lin Y, Gu F, Liang Z, Ding XF. A facile route to well-dispersed single-crystal silver nanoparticles from [AgSO3]− In water. J Alloys Compd 2011;509:7515-8.
21. Zhao Y, Chen A, Liang S. Shape-controlled synthesis of silver nanocrystals via γ-irradiation in the presence of poly (vinyl pyrrolidone). J Cryst Growth 2013;372:116-20.
22. Dong C, Zhang X, Cai H, Cao C. Facile and one-step synthesis of monodisperse silver nanoparticles using gum acacia in aqueous solution. J Mol Liq 2014;196:135-41.
23. Dong C, Zhang X, Cai H. Green synthesis of monodisperse silver nanoparticles using hydroxy propyl methyl cellulose. J Alloys Compd 2014;583:267-71.
24. Oluwafemi OS, Lucwaba Y, Gura A, Masabeya M, Ncapayi V, Olujimi OO, *et al.* A facile completely 'green' size tunable synthesis of maltose-reduced silver nanoparticles without the use of any accelerator. Colloids Surf B Biointerfaces 2013;102:718-23.
25. Raveendran P, Fu J, Wallen SL. A simple and "green" method for the synthesis of Au, Ag, and Au-Ag alloy nanoparticles. Green Chem 2006;8:34-8.
26. Magudapathy P, Gangopadhyay P, Panigrahi BK, Nair KG, Dhara S. Electrical transport studies of Ag nanoclusters embedded in glass matrix. Phys B 2001;299:142-6.
27. Sanghi R, Verma P. Biomimetic synthesis and characterisation of protein capped silver nanoparticles. Bioresour Technol 2009;100:501-4.
28. Rajan R, Chandran K, Harper SL, Yun SI, Kalaichelvan PT. Plant extract synthesized silver nanoparticles: An ongoing source of novel biocompatible materials. Ind Crops Prod 2015;70:356-73.
29. Rauwel P, Küünal S, Ferdov S, Rauwel E. A review on the green synthesis of silver nanoparticles and their morphologies studied via TEM. Adv Mater Sci Eng 2015;2015:9.
30. Irudaya Monisha S, Dayana Jeya Leela G, Anitha Immaculate A, Rosaline Vimala J. Comparative studies on yield and the phytochemical appraisal (Quality and Quantity) of *Manilkara hexandra* (Roxb) Dubarb using leaf, stem, and bark. J Pharmacogn Phytochem 2017;6:2052-8.
31. Yogendr M, Bahuguna. Dissertation; 2007.
32. Antony Lawrence A, Thomas Joseph Prakash J. Phytosynthesis: Physical and chemical characterization of silver nanoparticles using *Manilkara hexandra* (Roxb.) Dubard leaf extract and evaluation of antimicrobial and antioxidant potential. J Pharmacog Phytochem 2018;7:1634-44.
33. Bhattacharya D, Gupta RK. Nanotechnology and potential of microorganisms. Crit Rev Biotechnol 2005;25:199-204.
34. Abdel-Aziz MS, Shaheen MS, El-Nekeety AA, Abdel-Wahhab MA. Antioxidant and antibacterial activity of silver nanoparticles biosynthesized using *Chenopodium murale* leaf extract. J Saudi Chem Soc 2014;18:356-63.
35. Romero CD, Chopin SF, Buck G, Martinez E, Garcia M, Bixby L, *et al.* Antibacterial properties of common herbal remedies of the Southwest. J Ethnopharmacol 2005;99:253-7.
36. Farukh A, Ahmad I, Mehmood Z. Antioxidant and free radical scavenging properties of twelve traditionally used Indian medicinal plants. Turk J Biol 2006;30:177-83.
37. Darroudi M, Khorsand Zak M, Muhamad A, Huang MR, Hakimi NM. Green synthesis of colloidal silver nanoparticles by sonochemical method. Mater Lett 2012;66:117-20.
38. Siddiqui BS, Afshan F, Ghiasuddin, Faizi S, Naqvi SN, Tariq RM, *et al.* Two insecticidal tetranortriterpenoids from *Azadirachta indica*. Phytochemistry 2000;53:371-6.
39. Patel S, Sivaraj R, Rajiv P, Venckatesh R, Seenivasan R. Green synthesis of silver nanoparticles from the leaf extract of *Aegle marmelos* and evaluation of its antibacterial activity. Int J Pharm Pharm Sci 2015;7:169-73.
40. Shameli K, Bin Ahmad M, Jaffar Al-Mulla EA, Ibrahim NA, Shabanzadeh P, Rustaiyan A, *et al.* Green biosynthesis of silver nanoparticles using *Callicarpa maingayi* stem bark extraction. Molecules 2012;17:8506-17.
41. Sadeghi B, Gholamhoseinpoor F. A study on the stability and green synthesis of silver nanoparticles using Ziziphora tenuior (Zt) extract at room temperature. Spectrochim Acta A Mol Biomol Spectrosc 2015;134:310-5.
42. Ajitha B, Reddy YA, Reddy PS. Biogenic nano-scale silver particles by *Tephrosia purpurea* leaf extract and their inborn antimicrobial activity. Spectrochim Acta A Mol Biomol Spectrosc 2014;121:164-72.
43. Christy J, Dharaneya D, Vinmathi V, Justin Packia Jacob S. A green nano-biotechnological approach for the synthesis of silver nanoparticles using the seed coat of *Tamarindus indica*. Study of its antiba cterial and anticancer activity. Int J Pharm Pharm Sci 2015;7:192-4.
44. Anandalakshmi K, Venugobal J, Ramasamy V. Characterization of silver nanoparticles by green synthesis method using *Pedalium murex* leaf extract and their antibacterial activity. Appl Nanosci 2016;6:399-408.
45. Kalimuthu K, Suresh Babu R, Venkataraman D, Bilal M, Gurunathan S. Biosynthesis of silver nanocrystals by *Bacillus licheniformis*. Colloids Surf B Biointerfaces 2008;65:150-3.
46. Joshi SC, Kaushik U, Upadhyaya A, Sharma P. Green technology mediated synthesis of silver nanoparticles from *Momordica charantia* fruit extract and its bactericidal activity. Asian J Pharm Clin Res 2017;10:196-200.
47. Lin L, Qiu P, Cao X, Jin L. Colloidal silver nanoparticles modified electrode and its application to the electroanalysis of Cytochromec. Electrochimica Acta 2008;53:5368-72.
48. Sankar R, Karthik A, Prabu A, Karthik S, Shivashangari KS, Ravikumar V, *et al.* Origanum vulgare mediated biosynthesis of silver nanoparticles for its antibacterial and anticancer activity. Colloids Surf B Biointerfaces 2013;108:80-4.
49. Majeed Khan MA, Kumar S, Ahamed M, Alrokayan SA, Alsalhi MS. Structural and thermal studies of silver nanoparticles and electrical transport study of their thin films. Nanoscale Res Lett 2011;6:434.